Accepted for publication in Journal of Macromolecular Science Part B Physics
Published in May, 2016
DOI: 10.1080/00222348.2016.1197511

Comparative Properties of Styrene-Butadiene Rubbers (SBR) Containing Pyrolytic Carbon Black, Conventional Carbon Black and Organoclay

Running head: SBR with pyrolytic and industrial carbon black

P. Berki[1] and J. Karger-Kocsis[1,2*]

1- Department of Polymer Engineering, Faculty of Mechanical Engineering, Budapest University of Technology and Economics, H-1111 Budapest, Muegyetem rkp. 3, Hungary

2- MTA-BME Research Group for Composite Science and Technology, H-1111 Budapest, Muegyetem rkp. 3, Hungary

Authors' e-mails: karger@pt.bme.hu (*corresponding), berki@pt.bme.hu

Submitted to J. Macromol. Sci. Phys, February, and revised April 2016

ABSTRACT

To evaluate the reinforcing potential of pyrolytic carbon black styrene-butadiene rubber (SBR) was filled with pelletized pyrolytic carbon black (pCB_p), N660 industrial CB, their blend in a 1/1 ratio, and the latter also in the absence and presence of additional organoclay (OC). The Shore A hardness of the filled SBR gums was 65±2°. Effects of the compositions on the filler dispersion, cure behavior, dynamic mechanical thermal parameters (including the Payne effect), tensile mechanical (including the Mullins effect) and fracture mechanical (making use of the J-integral concept) properties were studied and discussed. Though pCB_p had a higher specific surface weight than CB, the latter proved to be a more active filler with respect to the tensile strength. The opposite tendency was found for the tear strength and fracture mechanics characteristics (J-integral at crack tip opening, tearing modulus and trouser tear strength). This was traced to an enlargement in the crack tip damage zone supported by the dispersion characteristics of the pCB_p. The performance of pCB_p was similar to that of CB with respect to some other properties. OC supported the filler networking which positively affected the resistance to crack initiation.

Key words:

styrene-butadiene rubber, carbon black, pyrolytic carbon black, mechanical properties, Payne effect, Mullins effect, J-integral, crack tip opening displacement

1. INTRODUCTION

The disposal and recycling of waste (worn, used, discarded) tires is a great challenge nowadays. Based on public concerns and legislative action ongoing research and developments works are addressing various recycling options of waste tires [1-2], focusing on obtaining valuable and commercializable products. Attempts were made to convert the ground tire rubber (GTR) into thermoplastic elastomers [2], reuse it alone [3] or in conventional rubber compounds [2,4]. It has been recognized, however, that the latter applications require – at least – partial devulcanization [2]. Promising approaches of industrial scale for devulcanization/reclaiming are related with ultrasonic [5] and microwave techniques [6-7]. Pyrolysis of waste tires is considered nowadays as an economic option [1,8]. Pyrolytic processes produce about 35 wt.% carbonaceous residues (also termed to as char, soot). Volatile or oily by-products can be used to as feedstock of the pyrolysis itself. Attempts have also been made to use the pyrolysis oil as an extender for rubber mixes [9]. The pyrolytic residue is composed of the original carbon black (CB), carbonaceous deposits and inorganic compounding fillers and vulcanizations aids (such as SiO_2 and ZnO, respectively) including their processing-related derivatives (ZnO transformed to ZnS). The composition, and also the type and amount of the carbonaceous depositions, depend on the actual feedstock (composition of the tire) and pyrolytic conditions [1, 8]. Provided that the feedstock is the same and the pyrolysis is conducted under well selected conditions, pyrolytic carbon black (pCB) in reproducible quality can be obtained. This pCB of controlled quality may be incorporated into tire and other rubber compounds thereby replacing – fully or partially – conventional CBs. The outcome of papers using pCBs of various origins in different rubber mixes is that their properties are closely matched with industrial reinforcing to semireinforcing furnace CBs in the range of N300 to N700 series [10-11].

Based on the above information this work was aimed at comparing the curing and mechanical properties of pCB and N660 type CB. Note that N660 is a semireinforcing CB widely used as filler in tire carcasses and sidewall recipes [12]. The selected fillers were incorporated at 60 part per hundred rubber (phr) amount, separately or in 1/1 ratio into and styrene-butadiene rubber (SBR). SBR was chosen because this rubber – together with natural rubber (NR) – are the essential blend components of tire recipes. Further, SBR should always be filled/reinforced due to the poor mechanical properties of the parent gum vulcanizate. This is the reason why the potential of pCB has mostly been checked in SBR- [11,13-14], and SBR/NR-based [9-10] mixes. A further aim was to check whether partial replacement of the dual black fillers (reduced to an overall amount 50 phr, pCB/CB=1/1) with organophilic modified clay (organoclay, added in 10 phr) can improve the properties of SBR. Note that organoclay (OC) – alone or in combination with CB – has been shown to be an excellent reinforcing additive in rubbers [15-

16]. Organoclays improved not only the mechanical performance but also other properties, such as flame retardancy and gas barrier properties, and even affected the curing [16]. To obtain a comprehensive picture about the potential of pCB_p in SBR the tests covered assessment of curing and filler dispersion, dynamic-mechanical thermal analysis (DMTA) and evaluation of the static tensile and static fracture mechanics behaviors.

2. EXPERIMENTAL

2.1.Materials

Characteristics of the pelletized pyrolytic carbon black (pCB_p) are given in Table 1. N660 CB (carbon content ≈ 99% (ASTM D 5291), specific surface: 35 m^2/g (ASTM D 6556-10), ash content: <0.7 % (ASTM D 1506), sulfur content: < 1% (ASTM D 3177)), serving for benchmarking, was provided by Tauril Co. (Hungary). Organoclay I.30 P (OC; Nanocor, USA) containing octadecylamine surfactant and having an initial intergallery distance of 2.1 nm, was used as further filler. As the rubber, SBR 1502 (styrene content: 23.5%, Money viscosity ML (1+4) at 100 ºC= 48 MU of Sterlitamak JSC, Russia), was selected. It was compounded with the fillers as indicated in Table 2.

Table 1: Major characteristics of the pCB_p used

Compositions, property	Method, standard	Unit	Value
Carbon content	ASTM D 5291	weight%	≈80
ZnO/ZnS content	estimated based on elemental analysis	weight%	≈7
SiO_2 content	-"-	weight%	≈13
Specific surface area (BET)	ASTM D 6556-10	m^2/g	≈75
Ash content	ASTM D 1506	weight%	≈22
Sulfur	ASTM D 3177	weight%	≈3

Table 2: Designation and composition of the SBR mixes. Note: since for comparison purpose it is recommended to keep the hardness of the rubbers constant [17], the carbon black filler content of the OC-containing rubbers was reduced while keeping the pCB_p/CB=1/1 ratio.

Designation	Composition [phr]							
	SBR	OC	CB (N660)	pCB_p	ZnO	Stearic acid	MBTS	S
SBRref	100	-	-	-	3	2	1.5	2
SBR/OC10	100	10	-	-	3	2	1.5	2
SBR/CB60	100	-	60	-	3	2	1.5	2
SBR/pCB_p60	100	-	-	60	3	2	1.5	2
SBR/pCB_p30-CB30	100	-	30	30	3	2	1.5	2
SBR/pCB_p20-CB20-OC10	100	10	20	20	3	2	1.5	2

2.2.Compounding and curing

The rubber was mixed on a laboratory two roll mill (LRM-SC-110, Labtech Engineering Co., Ltd., Thailand), friction was set to 1.3 and the temperatures of the front and back rotors were 70°C and 50°C, respectively. The additives were introduced in the time scale of 5-20 min after initiation of the mixing and the total time of mixing was 25 min. The samples were cured in a Teach-Line Platen Press 200E laboratory press (Dr. Collin GmbH, Germany) at 160°C for the $t_{0.9}$ time (time needed to reach 90% of cure in rheometer – see later) of the compounds with 5 MPa pressure, producing sheets with 2 mm thickness.

2.3.Testing

Curing

Curing studies were performed using a Monsanto R100S rheometer, (MonTech Werkstoffprüfmaschinen GmbH, Germany) in the isothermal time sweep mode (1,667 Hz, 1° angle) for the samples at T=160°C for 45 minutes.

Macrodispersion

Specimens were cut by a razor blade, embedded in polyester resin and afterward polished in three steps (coarse SiC, fine SiC and diamond suspension). Macrodispersion was assessed by an Olympus BX51M light microscope, equipped with a DP26 digital camera (Olympus GmbH, Germany) at 105x magnification in reflected light. The captured images (about ten per sample) were evaluated by the Olympus Stream software whereby accepting that particles with a diameter of >1 μm fall under the classification of macrodispersion. The dispersion coefficient was determined by dividing the overall surface of the macroparticles with the surface of the view field at this magnification and deducing it in percentage from 100%.

Dynamic-mechanical thermal analysis (DMTA)

DMTA spectra were registered on rectangular specimens in tensile mode at a static preload of 0.1 N with a superimposed sinusoidal 0.1% strain. The frequency was 10 Hz and the spectra were taken in a temperature range of -100 to 70°C using a Q800 device of TA Instruments Co. (USA). The temperature ramp was 3°C/minute. The DMTA technique was used to assess the Payne effect. It was also investigated in tensile mode, 0.01N static preload; however, at 30 °C using 10 Hz frequency with a strain sweep from 0.01 to 10% strain (denoted as M0.01 and M10, respectively).

Mechanical and fracture mechanical tests

Hardness was determined on the prepared sheets in ten parallel measurements on each material according to the DIN 53505 standard. A Zwick H04.3150 hardness tester (Zwick GmbH & Co. KG, Germany) was used with a Shore A measuring head using a 12.5 N load.

Specimens (DIN 53504 Type 1 for tensile and ASTM D624 Type C for tear tests) were punched from the sheets. Tensile and tear tests were performed on a Zwick Z250 universal testing machine equipped with a 20 kN load cell with a crosshead speed of 500 mm/min at room temperature. Each of above tests was repeated on five specimens to deduce the mean values. Strain softening (Mullins effect) was studied on the above dumbbell specimens which were loaded sequentially in five consecutive cycles to increasing strain levels, viz. to 50, 100 and 150 %, respectively. After reaching the lower fixed strain in the fifth cycle, the specimen was fully unloaded before starting with the subsequent loading cycle series up to the next, higher, fixed strain value. The Mullins effect was quantified as described later. The types of the specimens, and the fracture mechanics evaluation process are shown in Fig. 1.

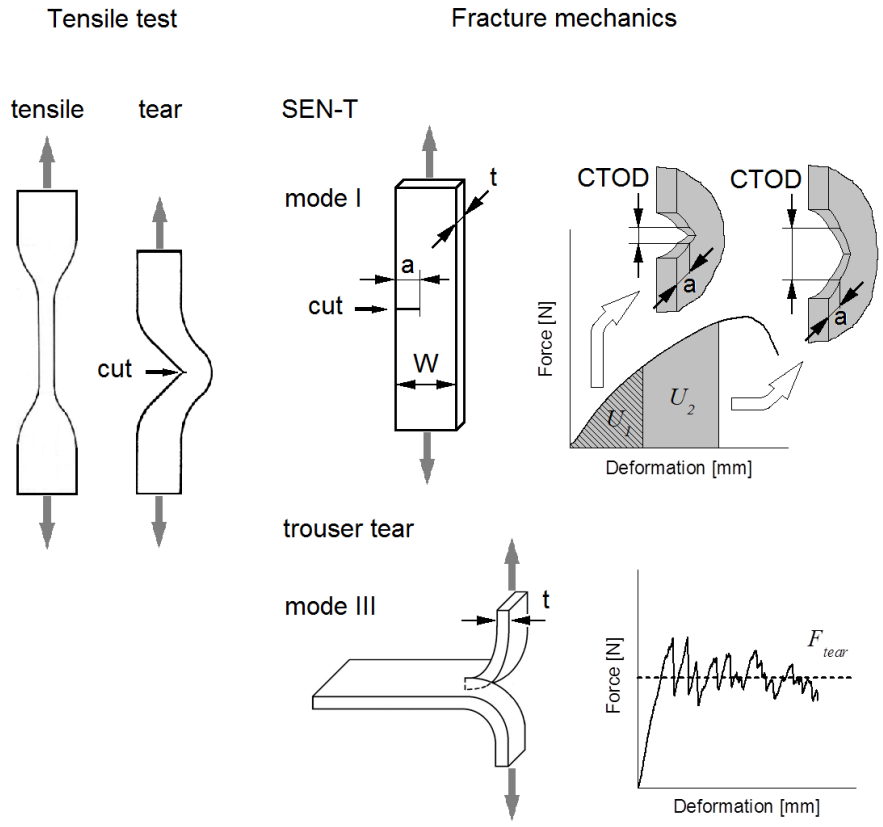

Figure 1: Types and designations of the specimens, and the data reduction process of the fracture mechanics treatise

Fracture mechanical tests were performed on single edge-notched tensile loaded (SEN-T) and trouser tear specimens. SEN-T specimens of 100 x 25 x 2mm dimension (length x width x thickness) with 10 mm initial notch length were loaded with 10 mm/min crosshead speed on the above mentioned Zwick testing machine. The crack tip opening displacement (CTOD) was followed by visual inspection using a digital miscroscope (Celestron 44302, USA). The camera was positioned in front of the crack in order to focus on the internal surface generated by

blunting and growing of the crack. Prior to this test the crack surfaces were coated by talc for contrast. By analyzing the registered sequence of pictures the point where fracture started to propagate could be detected and the corresponding J-integral value determined by [18]:

$$J = \frac{\eta \cdot U}{t \cdot (W - a)} \quad (1)$$

where η is a geometry factor (0.9 in this case), U is the input energy (given by the area under the load-displacement curve up to the point considered), t is the thickness (≈2 mm), W is the width (25 mm) of the specimen, and a is the initial crack length (10 mm)- cf. Fig. 1. J-integral tests were also performed on specimens which were loaded up to 100% deformation at 200 mm/min crosshead speed in five consecutive cycles (to eliminate the Mullins effect) and notched afterward. The J-integral was determined as a function of the crack tip opening displacement (CTOD) as shown schematically in Fig. 1. Further details of this test can be taken from Refs. [17-19].

The fracture energy from the trouser tear test ($J_{trouser}$) was determined on 100 x 30 x 2mm specimens (length x width x thickness) with an initial notch length of 40 mm at 100 mm/min deformation rate via Eq. 2 [20]:

$$J_{trouser} = \frac{2 \cdot F_{tear}}{t} \quad (2)$$

where F_{tear} is the mean force during stable tearing, and t is the specimen thickness- cf. Fig. 1. All fracture mechanics tests were also run on five parallel specimens.

3. RESULTS AND DISCUSSION

3.1.Cure behavior

Characteristic vulcanizations curves are displayed in Fig. 2 and the related results summarized in Table 3. The vulcametric data are: lowest and highest torque data (M_l and M_h, respectively), times to reach 10, 50 and 90% crosslinking ($t_{0.1}$, $t_{0.5}$ and $t_{0.9}$, respectively) and times to reach 1 and 2 dNm torque above the M_l torque value (t_{s1} and t_{s2}, scorch times). Based on Fig. 2 and Table 3 the following tendencies can be drawn: CB slightly accelerated the curing whereas pCB_p – also when combined with CB – had a marginal effect on it. OC had some accelerating effect; however, only when combined with CB and pCB_p. The first hint that SBR/pCB_p-CB-OC had similar hardness as SBR/pCB_p or SBR/CB was given by the similar M_h values (cf. Table 3).

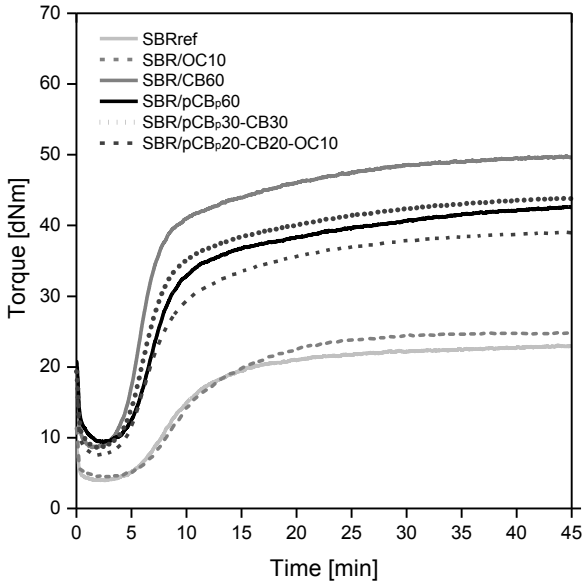

Figure 2: Vulcanization curves of the mixes tested

Table 3: Vulcanization results

Designation	M_l [dNm]	M_h [dNm]	$t_{0.1}$ [min]	$t_{0.5}$ [min]	$t_{0.9}$ [min]	t_{s1} [min]	t_{s2} [min]
SBRref	23.1	4.0	5.6	9.1	20.6	4.8	5.7
SBR/OC10	24.8	4.4	6.3	10.3	20.5	5.2	6.3
SBR/CB60	49.8	8.6	4.2	6.3	18.7	3.0	3.6
SBR/pCB_p60	42.7	9.4	5.1	7.6	23.7	4.1	4.5
SBR/pCB_p30-CB30	43.8	8.6	4.1	6.2	25.2	3.2	3.7
SBR/pCB_p20-CB20-OC10	39.2	8.2	4.0	6.4	18.0	3.3	3.7

3.2. Macrodispersion

Fig. 3 displays characteristic optical microscope pictures of the carbon black dispersions. The average sizes of the macroparticles were 3.3, 3.4 and 3.6 μm, and the dispersion coefficients 98, 85 and 88 % for SBR/CB60, SBR/pCB_p60 and SBR/pCB_p30-CB30, respectively. Accordingly, pCB_p was less dispersible than the industrial CB. It is noteworthy that the OC used became only slightly intercalated (ca. 0.2 nm expansion in the intergallery distance) in SBR, as shown earlier [21].

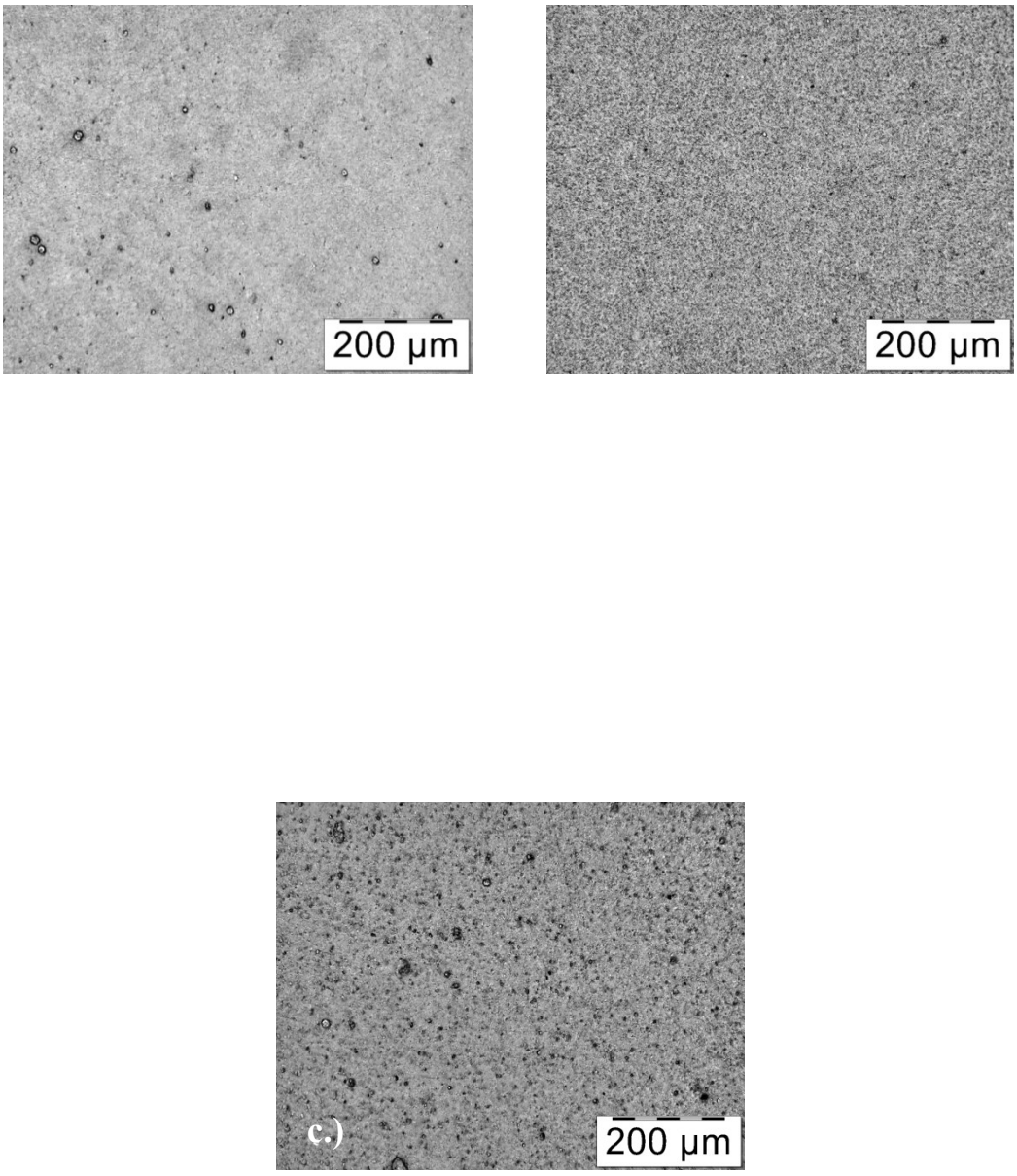

Figure 3: Characteristic light microscopic pictures taken from the polished surfaces of the SBR/CB60 (a), SBR/ pCB_p60 (b) and SBR/pCB_p30-CB30 (c)

3.3. DMTA behavior

Traces of the storage modulus (E') and mechanical loss factor (tan δ) as a function of the temperature are depicted in Figs. 4 a) and b), respectively. As expected, both the glassy and rubbery E' moduli increased with increasing filler content – see Fig. 4 a). On the other hand, a marginal change in the glass transition temperature (T_g), read at the temperature linked to the maximum of the tan δ peak, was found – cf. Fig. 4 b). In order to get a clearer picture about the different reinforcements, the rubbery E' moduli at T_g+30 °C ($E_{rubbery}$), and the glassy ones (E_{glassy}) at T_g-30°C were read and are tabulated in Table 4. $E_{rubbery}$ was used to calculate the apparent crosslink density, more exactly the apparent mean molecular weight between crosslinks, via:

$$M_c = \frac{3\rho \cdot R \cdot T}{E_{rubbery}} \quad (3)$$

where $E_{rubbery}$ is the modulus at $T=T_g + 30K$, ρ is the density (determined in a pycnometer using methanol), R is the universal gas constant (8.314 J/(K.mol), and T is the absolute temperature. Recall that M_c is an apparent value because in the filled rubbers it involves not only their crosslinking but the rubber–filler and filler–filler interactions. Based on increasing crosslink density (decreasing M_c) values the ranking of the SBRs were as follows:

SBR ref.< SBR/OC10<SBR/pCB_p30-CB30<SBR/CB60≈SBR/pCB_p60<SBR/pCB_p20-CB20-OC10

This ranking only slightly changed when the reduction in the maximum of the tan δ is considered (cf. Fig. 4 b) and data in Table 4). Increasing reinforcing effectiveness is associated with decreasing tan δ values because the segmental motion of the rubbers chains is hampered in the filler-rubber interphase.

The Payne effect is related to the formation of a filler (or secondary) network [22]. CB aggregates form agglomerates owing to van der Waals interactions between them. Since the van der Waals forces act in a short range the onset and magnitude of the Payne effect informs us about the agglomeration tendency, and thus on the reinforcing activity of the given carbon black. This is a crucial issue for pCB due to its peculiar composition along with the fact that the carbonaceous deposition, covering the pyrolysis residue, is of amorphous nature. By contrast, standard CBs are more crystalline and the crystallization during production dictates the surface appearance, as well [11]. Fig. 5 shows the Payne effect in the investigated strain range for the SBR gums. It is quantified by the difference in the E' moduli measured at 0.01 and 10% strains (denoted as M0.01-M10 in analogy to the tensile moduli - see below), respectively. This difference is marginal for SBR, which is in line with the corresponding model [22]. The Payne effect is somewhat higher for pCB_p than for CB at 60 phr filling. Usually, with increasing specific surface weight of CB the related Payne effect increases, as well. Though the scenario is more complex, this finding is in harmony with the BET surface values in section 2.1 (cf. Table 1). The combined use of pCB_p and CB yields the same effect as that of CB alone.

OC, when added even only at 10 phr, proves to be an efficient networking filler itself (cf. Figure 5). When OC is combined with pCB_p and CB then a synergetic effect appears – cf. Fig. 5 and Table 4. Further information on the reinforcing efficiency of the fillers can be deduced when considering the ratio of the maximum in the loss modulus (E'') to the measured Payne effect (i.e. M0.01-M10) – cf. Table 4. The higher this value the more active the actual filler is [11]. Data in Table 4 show that CB has higher activity than pCB_p. As expected, the combined use of them yielded an intermediate value.

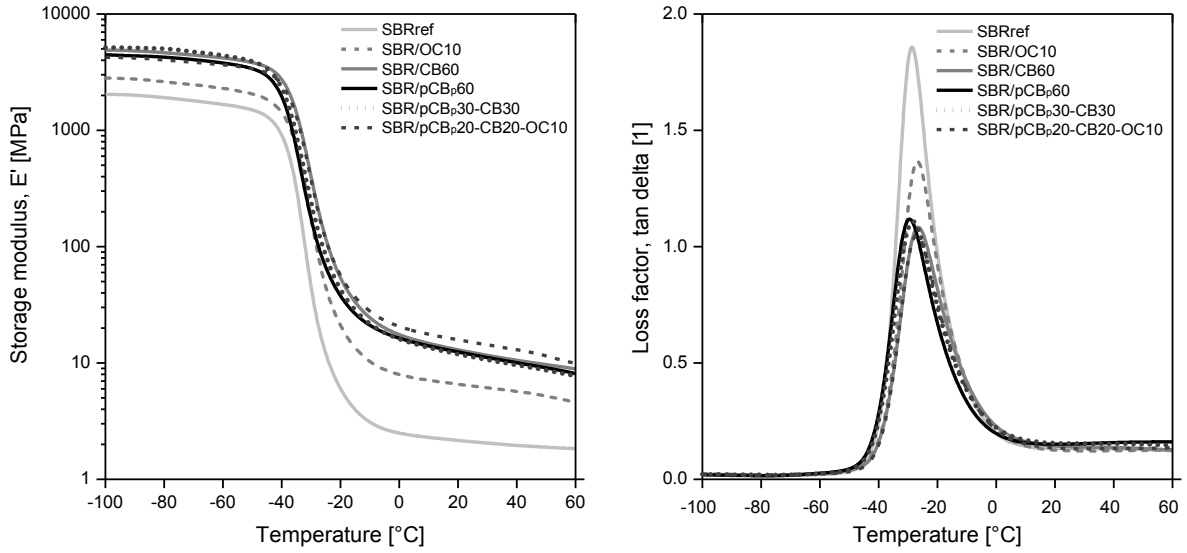

Figure 4: a) Storage modulus (E') and b) mechanical loss factor (tan δ) as a function of temperature for the SBR systems studied

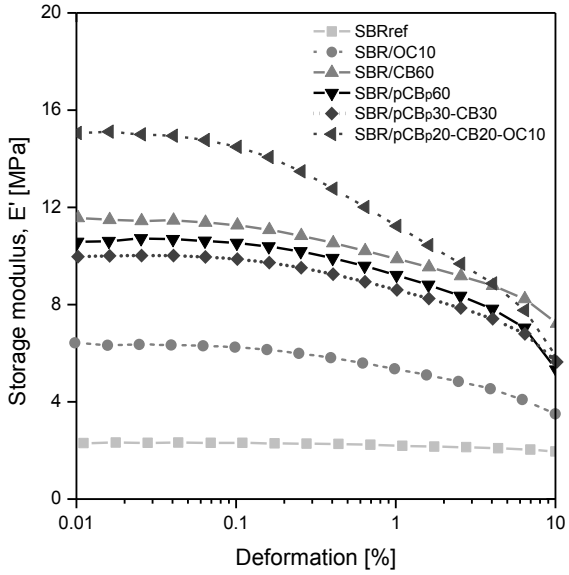

Figure 5: E' as a function of strain (Payne effect) for the SBR gums tested

Property [unit]	SBRref	SBR/OC10	SBR/CB60	SBR/pCB$_p$60	SBR/pCBp30 -CB30	SBR/pCBp20 -CB20-OC10
Density [g/cm^3]	0.992	1.130	1.282	1.244	1.263	1.279
M_c [g/mol]	3445	1291	753	762	811	614
T_g [°C]	-28.7	-26.8	-26.5	-29.6	-28.3	-27.0
tan δ at T_g [1]	1.86	1.37	1.08	1.12	1.11	1.05

E'_{glassy} (T_g-30°C) [MPa]	1650	2230	4080	3780	4330	3590
$E'_{rubbery}$ (T_g+30°C) [MPa]	2.5	7.6	16.3	16.2	15.5	19.5
Payne effect, M0.01-M10 [MPa]	0.34	2.93	4.35	5.26	4.34	9.24
E''_{max} [MPa]	0.32	0.78	1.65	1.66	1.52	2.01
E''_{max} /(M0.01-M10) [1]	N/A	0.27	0.38	0.32	0.35	0.22

Table 4: Density and DMTA-related properties of the filled SBR systems

3.4. Mechanical behavior

Characteristic tensile strength vs. strain curves along with the corresponding data are displayed in Fig. 6, and also tabulated in Table 5. Table 5 lists also the Shore A hardness values. Recall that our attempt was to keep the Shore hardness values for the filled SBRs comparable. This was the reason why pCB and CB were added at 20 phr each when OC was introduced at 10 phr as a further "networking" filler. One can notice in Fig. 6 that the highest tensile strength accompanied with the lowest tensile elongation of the filled samples was shown by SBR-CB60. Conversely, lower tensile strength and higher ductility were found for SBR/pCB_p suggesting that pCB_p60 is a less active filler than CB irrespective of the fact that the BET surface of pCB_p is higher than that of CB. Their combined use in 1/1 ratio yields intermediate results. The strength data of the recipe containing pCB_p, CB and OC at 20, 20 and 10 phr, respectively, were slightly better than with 60 phr pCB_p.

In order to have an impression of the shape of the stress-strain curves, the strength data at 50, 100, 200 and 300% strains (termed as to moduli, M50, M100, M200 and M300, respectively) are depicted in Fig. 7. It is noteworthy that SBR/pCBp20-CB20-OC10 behaved similarly to SBR/pCBp60 though the former contained 10 phr less filler amount.

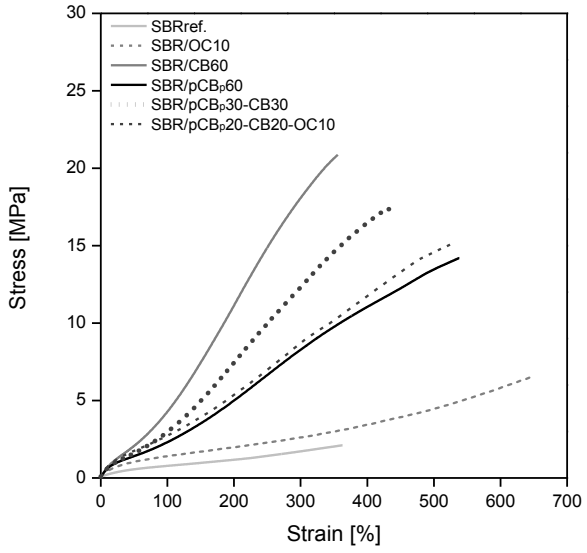

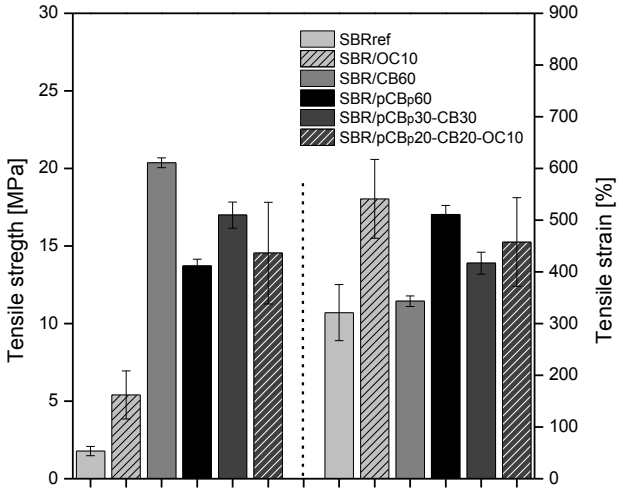

Figure 6: a) Characteristic stress-strain curves, and b) tensile characteristics for the SBR samples studied

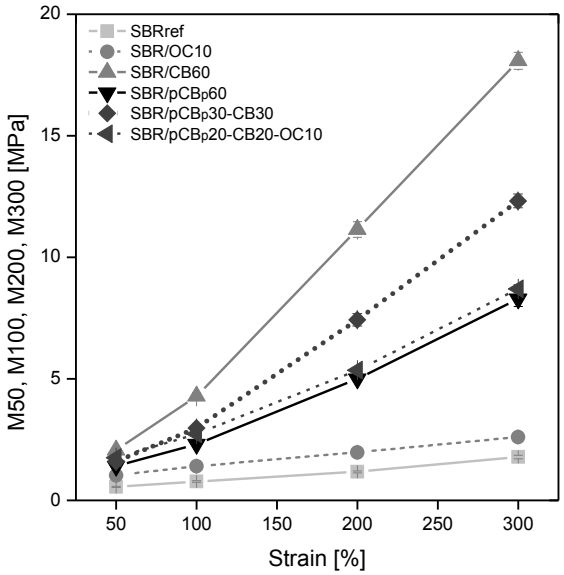

Figure 7: Moduli at different strains for the SBR systems studied

The sketch in Fig. 8 shows how the Mullins effect in this work has been considered. The Mullins effect was quantified by considering the force ratio of the cyclic (in five consecutive cycles denoted by F1 to F5) and separate monotonic loading (F0) of the specimens to a given strain as a function of the loading cycles (1 to 5). The change in the dissipated energy (E_{diss}) was considered in a similar way, i.e. the hysteresis was related to the overall energy introduced (cf. Fig. 8) [17]. The corresponding data are also listed in Table 5.

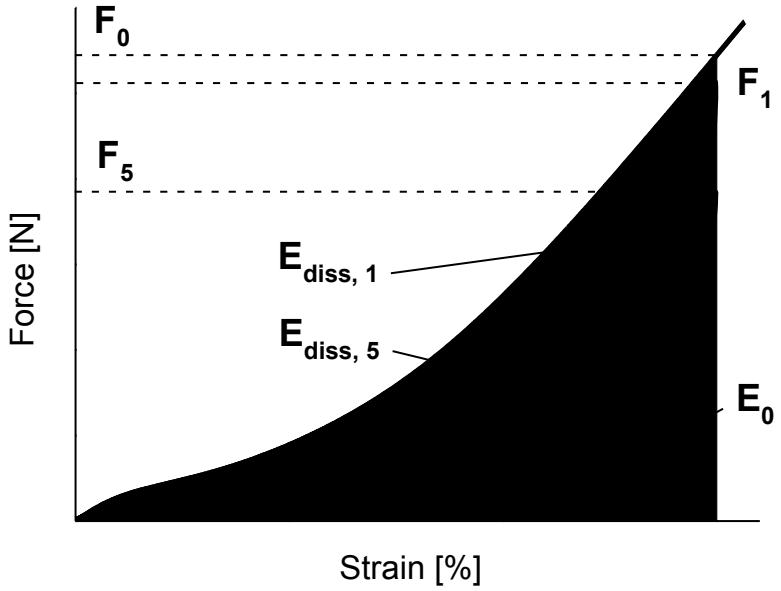

Figure 8: Mullins effect and its quantification schematically

The Mullins effect was very similar for both pCB_p and CB. As expected, the largest softening occurred in the first cycle. This effect was strain sensitive practically for all samples (cf. Table 5).

Interestingly, pCB_p outperformed CB at 60 phr with respect to the tear strength. The positive effect of pCB_p remained also when combined with CB (Fig. 9). This can be attributed to a coarser dispersion of pCB_p than CB. A bimodal dispersion of fillers (which may be different with respect to chemical composition and aspect ratio) often yields an improvement in the tear strength [23-24]. This should be traced to the onset of a zig-zag type fracture path which is accompanied with higher energy dissipation [23]. A strong improvement in the tear strength was expected by the incorporation of OC due to its high aspect ratio favoring the crack deflection mechanism (the appearance of which is the zig-zag-type pattern). This was, however, not the case, suggesting that the overall amount of fillers had a larger effect than the filler aspect ratio on this parameter.

Property [unit]	SBRref	SBR/OC10	SBR/CB60	SBR/pCB_p60	SBR/pCBp30 -CB30	SBR/pCBp20 -CB20-OC10
Shore A [°]	40±0	50±1	67±1	63±1	63±1	65±0
M-50 [MPa]	0.6±0.0	1.0±0.0	2.1±0.1	1.4±0.0	1.6±0.0	1.8±0.0
M-100 [MPa]	0.8±0.0	1.4±0.1	4.3±0.1	2.3±0.1	3.0±0.1	2.7±0.1
M-200 [MPa]	1.2±0.0	2.0±0.1	11.1±0.3	5.0±0.1	7.4±0.3	5.4±0.1
M-300 [MPa]	1.7±0.1	2.6±0.1	18.1±0.4	8.3±0.3	12.3±0.3	8.7±0.2
Tensile strength [MPa]	1.9±0.1	5.4±1.5	20.4±0.3	13.7±0.4	17.1±0.8	16.0±1.0
Tensile strain [%]	345±14	541±76	343±10	511±18	417±21	495±26

Tear strength [kN/m]		5.4±0.1	7.5±0.7	16.8±1.1	26.6±1.8	19.6±1.3	13.9±0.6
Mullins-effect [%]	$F_{max.\ 50.\ 1}$	85±1	93±3	92±5	93±2	88±3	86±2
	$F_{max.\ 50.\ 5}$	83±1	87±3	90±5	88±2	83±3	81±1
	$F_{max.\ 150.\ 1}$	92±2	97±2	97±6	95+3	95±4	91±1
	$F_{max.\ 150.\ 5}$	90±2	91±2	92+4	85±3	83±3	81±1
	$E_{diss.\ 50.\ 1}$	8±2	16±1	20±2	19±1	18±3	17±1
	$E_{diss.\ 50.\ 5}$	6±2	9±2	13±2	12±0	11±2	12±0
	$E_{diss.\ 150.\ 1}$	6±1	20±0	35±3	34±1	24±1	25±0
	$E_{diss.\ 150.\ 5}$	5±1	10±1	14±1	12±0	10±1	11±0

Table 5: Hardness, tensile mechanical parameters, tear strength and Mullins effect for the filled SBR samples. Note: Mullins effect is given only for the 50 % and 150 % deformations by codes $F_{\text{max strain (\%). cycle (number)}}$ and $E_{\text{diss strain (\%). cycle (number)}}$

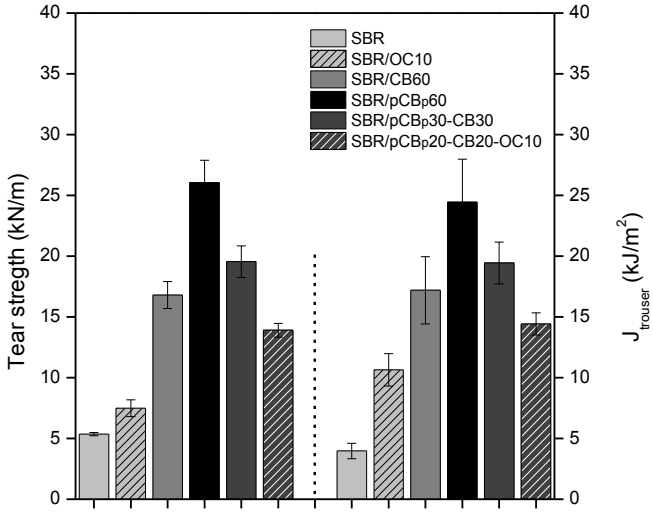

Figure 9: Tear strength and $J_{trouser}$ values for the SBR mixes

3.5. Fracture mechanics results

Characteristic J-integral vs. CTOD traces of the specimens with and without cyclic preloading are shown in Fig. 10 and the related results summarized in Table 6. The critical value of the J-integral (J_c) is usually traced to the crack onset. Because it can be hardly resolved optically, the J-integral value at CTOD=0.5 mm was taken as J_c value. In this respect we have followed the recommendations of Ref. [18]. Cyclic preloading markedly reduced the J_c data (cf. Table 6) confirming effect of Mullins strain softening.

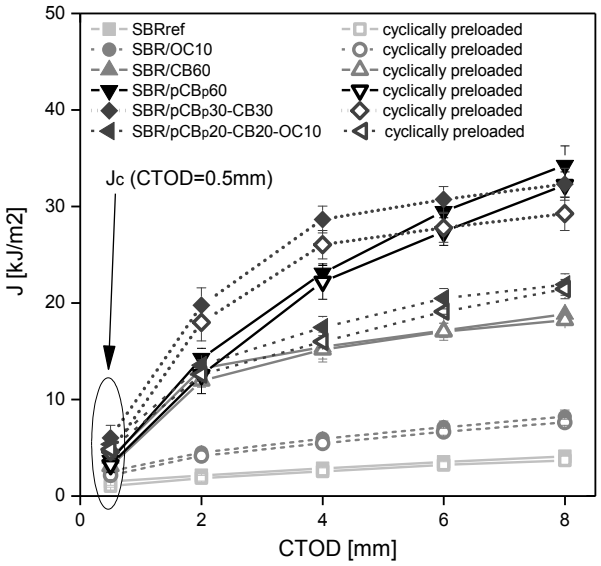

Figure 10: J-integral as a function of crack tip opening displacement (CTOD) for the SBR mixes. Notes: this figure also shows the reading of the J_c at CTOD=0.5mm. The tearing modulus is given as the slope of the J vs. CTOD curves in the CTOD range 0.5 to 2 mm.

Property [unit]	SBRref	SBR/OC10	SBR/CB60	SBR/pCB$_p$60	SBR/pCBp30 -CB30	SBR/pCBp20 -CB20-OC10
$J_{critical.\ CTOD*=0.5mm}$ [kJ/m^2]	1.49±0.20	2.55±0.18	3.93±0.30	3.69±0.39	6.00±0.32	5.37±0.27
$J_{critical.\ CTOD*=0.5mm}$ cyclically preloaded [kJ/m2]	1.02±0.09/ -31.5%	2.35±0.25/ -7.8%	3.09±0.30/ -21.4%	3.22±0.34/ -12.7%	4.55±0.49/ -24.2%	4.84±0.27/ -9.9%
Tearing modulus, T_J [MJ/m^3]	0.68	1.28	6.19	7.06	9.18	5.45
Tearing modulus, T_J cyclically preloaded [MJ/m^3]	0.44/ -35.3%	1.24/ -3.1%	5.91/ -4.5%	6.23/ -11.8%	8.95/ -2.5%	5.16/ -5.3%
J_{total} [kJ/m^2]	5.70±0.41	14.30±1.56	23.58±1.94	48.82±2.18	36.24±2.62	24.06±1.97
J_{total}, cyclically preloaded [kJ/m^2]	5.50±0.38/ -3.5%	13.14±1.14/ -8.1%	21.95±0.70/ -6.9%	45.16±2.45/ -7.5%	33.45±2.54/ -7.7%	23.24±1.54 -3.4%
$J_{trouser}$ [kJ/m^2]	3.97±0.64	10.64±1.34	17.19±2.77	24.45±3.52	19.44±1.73	14.42±0.91

Table 6: Fracture mechanical parameters of the SBR gums tested. Notes: J_{total} represents a specimen-related toughness, namely the energy required to break a notched specimen in tensile loading. The property degradation owing to preloading (Mullins effect) is indicated in percentage

The combined use of pCB$_p$ and CB had a synergistic effect on the J_c, also when OC was present. This means that the resistance to crack formation was markedly enhanced. It is hypothesized

that an efficient stress redistribution via the fillers' dispersion occurred during crack blunting and onset. This should be accompanied with an enlargement of the damage zone that could be verified by in-situ loading of the specimens in a scanning electron microscope (in progress). The synergism remained also for the tearing modulus, however, only in case of SBR/pCB_p30-CB30. This suggests that either the size of the damage zone and/or the energy absorbing mechanisms (debonding with molecular stretching) within were changing during the crack propagation.

Values of $J_{trouser}$ were much higher than J_c (cf. Table 6). On the other hand, $J_{trouser}$ data matched very well with those of the tear strength (cf. Fig. 9) although the former is linked with mode III-type (tearing), whereas tear strength is related to mode I (crack tip opening) type loading – cf. Fig. 1. Note their units are the same when kJ/m^2 is used instead of the traditional kN/m (steady force in the test divided by the thickness of the corresponding specimen) for the tear test. This agreement suggests that even in trouser tear a mode I-type loading prevails in the root of the crack tip. If this explanation holds then what is the reason for the large difference between J_c and $J_{trouser}$? This can be traced to the fact that $J_{trouser}$ is related to crack propagation (recall that F_{tear} in Equation 2 was read as the mean value of stable tearing – cf. Fig. 1) while J_c (CTOD=0.5 mm) refers to crack initiation.

4. CONCLUSIONS

This work was devoted to check the potential of using pelletized pyrolytic carbon black (pCB_p) as reinforcing filler in SBR. SBR compounds of the same hardness were produced by filling with pCB_p, industrial N660 type CB and their blend in a 1/1 ratio. In case of the pCB_p/CB blend the effect of additional organoclay (OC) was also considered. Based on the results obtained the following conclusions can be drawn:

- pCB_p is less dispersible than CB. Its incorporation into SBR does not affect the curing. Based on DMTA results CB is only a slightly more active filler than pCB_p. OC acted as a "networking" filler when the SBR was loaded with pCB_p and CB together.
- CB yielded higher tensile strength and lower elongation at break than pCB_p confirming its higher reinforcing activity. On the other hand, the tear strength with pCB_p, even when combined with CB, was higher than with CB alone. This was attributed to the favorable effect of the dispersion (in macro-, micro- and nanoscale) of pCB_p.
- synergistic effects with respect to crack initiation (J_c) and growth (T_j) were observed for the common use of pCB_p and CB. It was traced to effects of the fillers' dispersion, supporting an efficient stress transfer/relieve locally, thereby enlarging the related damage zone. Related data on SBR/pCB_p-CB-OC supported this hypothesis. $J_{trouser}$ agreed with the tear strength suggesting that even under mode III-type loading, mode I, i.e. crack opening, conditions prevailed.

References:

1. Martínez, J. D.; Puy, N.; Murillo, R.; García, T.; Navarro, M. V.; Mastral, A. M. Waste tyre pyrolysis – A review. Renew. Sust. Energy Rev., **2013**, 23, 179-213.
2. Karger-Kocsis, J.; Mészáros, L.; Bárány, T. Ground tyre rubber (GTR) in thermoplastics, thermosets, and rubbers. J. Mater. Sci., **2013**, 48, 1-38.
3. Formela, K.; Klein, M; Colom, X.; Saeb, M. R. Investigating the combined impact of plasticizer and shear force on the efficiency of low temperature reclaiming of ground tire rubber (GTR). Polym. Degr. Stab., **2016**, 125, 1-11.
4. Formela, K.; Haponiuk, J. T. Curing characteristics, mechanical properties and morphology of butyl rubber filled with ground tire rubber (GTR). Iran Polym. J., **2014**, 23, 185-194
5. Isayev, A. I.; Liang, T.; Lewis, T. M. Effect of particle size on ultrasonic devulcanization of tire rubber in twin-screw extruder. Rub. Chem. Technol., **2014**, 87, 86-102.
6. Garcia, P. S.; de Sousa, F. D. B.; de Lima, J. A.; Cruz, S. A.; Scuracchio, C. H. Devulcanization of ground tire rubber: Physical and chemical changes after different microwave exposure times. Express Polym. Lett., **2015**, 9, 1015-1026.
7. Seghar, S.; Ait Hocine, N.; Mittal, V.; Azem, S.; Al-Zohbi, F.; Schmaltz, B.; Poirot, N. Devulcanization of styrene butadiene rubber by microwave energy: Effect of the presence of ionic liquid. Express Polym. Lett., **2015**, 9, 1076-1086.
8. Williams, P. T. Pyrolysis of waste tyres: A review. Waste Manag., **2013**, 33, 1714-1728.
9. Karabork, F.; Tipirdamaz, S. T. Influence of pyrolytic carbon black and pyrolytic oil made from used tires on the curing and (dynamic) mechanical properties of natural rubber (NR)/styrene-butadiene rubber (SBR) blends. Express Polym. Lett., **2016**, 10, 72-82.
10. Cataldo, F. Preparation of pyrolytic carbon black from scrap tire rubber crumb and evaluation in new rubber compounds. Macromol. Mater. Eng., **2005**, 290, 463-467.
11. Norris, C. J.; Hale, M.; Bennett, M. Pyrolytic carbon: factors controlling in-rubber performance. Plast. Rub. Compos., **2014**, 43, 245-256.
12. Medalia, A. I. Carbon black In *Mixing and Compounding of Polymers: Theory and Praxis*; Manas-Zloczower, I.; Tadmor, Z. Eds.; Hanser:Munich, 1994; 493-519.
13. Du, A.; Wu, M.; Su, C.; Chen, H. The characterization of pyrolytic carbon black prepared from used tires and its application in styrene-butadiene rubber (SBR). J. Macromol. Sci. Part B, Phys., **2008**, 47, 268-275.
14. Delchev, N.; Malinova, P.; Mihaylov, M.; Dishovsky, N. Effect of the modified solid product from waste tyres pyrolysis on the properties of styrene-butadiene rubber based composites. J. Chem. Technol. Metallurgy, **2014**, 49, 525-534.
15. Teh, P. L.; Mohd Ishak, Z. A.; Hashim, A. S.; Karger-Kocsis, J.; Ishiaku, U. S. On the potential of organoclay with respect to conventional fillers (carbon black, silica) for epoxidized rubber compatibilized natural rubber vulcanizates. J. Appl. Polym. Sci., **2004**, 94, 2438-2445.
16. Galimberti, M. Ed., *Rubber-Clay Nanocomposites*, Wiley:Hoboken, 2011.

17. Padenko, E.; Berki, P.; Wetzel, B.; Karger-Kocsis, J. Mechanical and abrasion wear properties of hydrogenated nitrile butadiene rubber of identical hardness filled with carbon black and silica. J. Reinf. Plast. Compos., **2016**, 35, 81-91.
18. Ramorino, G.; Agnelli, S.; De Santis, R.; Riccò, T. Investigation of fracture resistance of natural rubber/clay nanocomposites by J-testing. Eng. Fract. Mech., **2010**, 77, 1527-1536.
19. Agnelli S.; Ramorino, G.; Passera, S.; Karger-Kocsis, J.; Riccò, T. Fracture resistance of rubbers with MWCNT, organoclay, silica and carbon black fillers as assessed by the J-integral: Effects of rubber type and filler concentration. Express Polym. Lett., **2012**, 6, 581-587.
20. Gent, A. N.; Mars, W. V. Strength of elastomers In *The Science and Technology of Rubber*, Mark, J.E.; Erman, B.; Roland C.M. Eds.; Academic Press:Waltham, 2013, 473-516.
21. Mousa, A.; Karger-Kocsis, J. Rheological and thermodynamical behavior of styrene/butadiene rubber-organoclay nanocomposites. Macromol. Mater. Eng., **2001**, 286, 260-266.
22. Heinrich, G.; Vilgis, T. A. A statistical mechanical approach to the Payne effect in filled rubbers. Express Polym. Lett., **2015**, 9, 291-299.
23. Gatos, K.G.; Sawanis, N.; Apostolov, A. A.; Thomann, R.; Karger-Kocsis, J. Nanocomposite formation in hydrogenated nitrile rubber (HNBR)/organo-montmorillonite as a function of intercalant type. Macromol. Mater. Eng., **2004**, 289, 1079-1086.
24. Chen, W.J.; Gu, J.; Xu, S. H. Exploring nanocrystalline cellulose as a green alternative of carbon black in natural rubber/butadiene rubber/styrene-butadiene rubber blends. Express Polym. Lett., **2014**, 8, 659-668.